Mendil *et al. EURASIP Journal on Wireless Communications and Networking* (2017) 2017:127
DOI 10.1186/s13638-017-0913-4

EURASIP Journal on Wireless Communications and Networking

RESEARCH Open Access

Battery aging-aware energy management of green small cells powered by the smart grid

Mouhcine Mendil[1,2*], Antonio De Domenico[1], Vincent Heiries[1], Raphael Caire[2] and Nouredine Hadjsaid[2]

Abstract

Mobile operators are deploying energy-harvesting heterogeneous networks due to their foreseen advantages such as self-sustainable capability and reduced operating expenditure, which cannot be offered by conventional grid powered communications. However, the used energy storage is subject to irreversible aging mechanisms, requiring intelligent management that considers both the energy cost and battery life cycle. In this paper, we propose a cognitive energy management strategy for small cell base stations powered by local renewable energy, a battery, and the smart grid to simultaneously minimize electricity expenditures of the mobile operators and enhance the life span of the storage device. Non-linear battery models and aging processes are considered to formulate the energy cost optimization problem. Simulation results in different configurations show that a degradation-aware policy significantly improves the battery lifetime, while achieving considerable cost savings.

Keywords: Cognitive energy management, Green communication, Energy harvesting, Small cell, Battery, Smart grid

1 Introduction

In the last decades, mobile user density and data traffic volume have exponentially increased all over the world. To respond to this trend, the mobile network operators (MNOs) have deployed small cell base stations (SBSs) to enhance their network service capabilities [1]. According to [2], this solution results in a significant energy demand augmentation essentially generated by the base station power consumption that represents 75 to 80% of the entire mobile network. Based on this, the deployment of heterogeneous cellular networks (HetNets) requires an efficient energy management to ensure their economic and environmental sustainability.

A multitude of concepts have recently been proposed to improve the energy efficiency in wireless communications, addressing network planning, protocols, and equipments [3]. In addition, renewable energy (RE) usage in cellular networks has drawn attention for its numerous benefits such as decreasing carbon emissions, enabling long-term cost savings thanks to reduced operating expenditure (opex) [4], and feeding off-grid base stations where the connection to the power grid is expensive or impossible [5]. In this context, cognitive techniques have been explored to improve energy-harvesting communications [6]. More specifically, the cognitive radio offers the ability to sense the conditions of the wireless communication networks and interact with the environment to adjust some parameters such as the transmission power, frequency band, and modulation mode [7].

The current energy-harvesting technologies require local energy storage to absorb the production fluctuation and ensure a continuous equilibrium between energy offer and demand. However, the typical used energy storage, i.e., electric battery, generates expensive investment cost and is subject to irreversible degradations. Such phenomenon, called battery aging, has been intensively studied and been classified into two categories: cycle aging, which is due to the energy exchanges with the battery, and calendar aging that appears when the battery is on rest [8]. In this context, Barre et al. [9] have presented a comprehensive review of techniques, models, and algorithms used for Li-ion battery aging estimation.

The presence of energy storage requires intelligent energy management policies to optimize the energy cost of grid-connected base stations (BSs) with energy harvesting. Some studies in the literature have addressed this problem by using either offline or online optimization

*Correspondence: mouhcine.mendil@gmail.com
[1]CEA, LETI, MINATEC, F-38054, Grenoble, France
[2]University Grenoble Alpes, G2Elab, F-38054, Grenoble, France

approaches. The first category assumes perfect knowledge of the stochastic energy variables [10–12]. In [11] for example, the power consumption of a HetNet powered by RE and equipped with an infinite-capacity battery has been optimized by supervising the BS transmit power and the battery usage. In particular, non-linear model predictive control theory has been used to manage the stored energy considering the average electricity price and power production. Zhang et al. [12] have proposed an energy-aware traffic offloading for a HetNet with multiple SBSs. They have used queuing theory to model the energy production and consumption and deduced an efficient power control according to the statistical information of energy arrival and traffic load. Online policies have also been proposed by assuming a casual knowledge of the environment. In this context, stochastic optimization has been implemented by assuming that the statistics of the energy processes are known and that past observations can correct the energy forecasts [13–15]. The authors in [13] have investigated an online stochastic approach based on multi-period recourse. Mao et al. [15] have considered a hybrid energy supply for the HetNet and formulated the energy cost minimization problem as a discrete Markov decision process. The monotony properties of the optimal policy have been inferred to simplify and solve the optimization problem using the backward induction algorithm. In [16], we have proposed an energy controller that uses reinforcement learning techniques to elaborate an optimal energy flow policy without prior knowledge of the environment stochastic behavior.

These works have focused on maximizing the energy saving, and none has integrated both calendar and cycle battery agings in the energy management framework. As a matter of fact, the maximal use of the battery flexibility enables large cost savings but can lead to rapid battery life loss. However, the battery is an expensive investment of the system, and enhancing its life span is vital for an efficient return on investment. Consequently, there is a trade-off between pure cost-efficient and battery aging-aware strategies that has not been evaluated so far. This motivated us to investigate the design of a cognitive energy controller that optimizes the operating energy cost while using the battery in the most effective way to avoid accelerated cycle and calendar agings. The current study extends our work [17] by introducing the battery aging models and formulating the energy cost problem such that the battery degradation factors are reduced while the optimal cost saving is still achieved. Additionally, the battery life evolution is studied to show the impact of the proposed energy strategies on the aging process.

1.1 Contributions and organization

The contributions of this paper are summarized as follows:

- Different from existing works, we propose a cognitive energy flow management framework for grid-connected energy-harvesting SBSs to jointly optimize the energy opex and the battery life cycle. The cognitive decision architecture is centered around the battery and uses realistic models to capture the non-linear battery behavior and aging mechanisms. Without loss of generality, the present framework is implemented in the offline case, in which we consider non-casual information about the environment variables. System simulations show that the proposed controller achieves considerable cost reduction compared to simpler strategies.
- The trade-off between pure energy cost optimization and battery aging-aware policies is explored. The energy cost and battery aging are evaluated in different configurations. Simulation results show that the proposed energy management allows considerable battery life extension such that the battery lasts five times longer compared to a pure energy cost optimization strategy. In exchange, the opex is slightly increased but this additional expense remains negligible with respect to the current battery replacement cost.

The paper is structured as follows. Section 2 introduces our proposed architecture and the associated system models. Section 3 provides a formulation of the joint cost minimization and battery life preservation problem for a green small cell. Section 4 presents the simulation results. The paper is concluded and perspectives are discussed in Section 5.

2 System architecture

The proposed architecture, illustrated in Fig. 1, is composed of:

- The SBS: wireless communication station covering a small area (10 m to 1 km), used to offer high data rate services to mobile users.
- The photo-voltaic (PV) system: equipment harvesting solar energy to produce electricity. It is one of the two energy sources of the system.
- The two-way link to the smart grid (SG): the SG is the second energy source of the system. The two-way energy connection enables to buy or sell electricity to the power grid.
- The battery: storage device that offers flexibility in the energy utilization. It can store the electricity coming from the SG and the PV system to feed the SBS or sell the energy back to the SG.
- The cognitive energy supervision system (ESS): controller that schedules the energy flows to reduce the electricity bill and improve the battery life span.

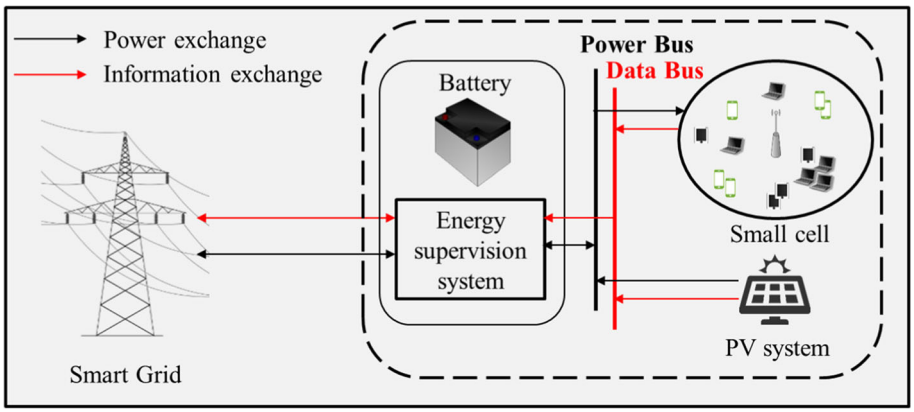

Fig. 1 System architecture of the proposed cognitive energy supervisor for small cells

In the following, we present the chosen model for each component of the system.

2.1 Small cell base station power consumption model

The SBS load ρ is modeled as a non-homogeneous Poisson process, whose intensity varies during time. We suppose that, depending on the load, the SBS can operate in two modes: active when $\rho > 0$ and sleep when $\rho = 0$. The relation between the SBS power consumption P_{BS} [W] and the traffic load is given by the following equation [18]:

$$P_{\mathrm{BS}}(t) = \begin{cases} P_0 + \Delta_{\mathrm{p}} \cdot \rho(t) \cdot P_{\max}, & \text{if } 0 < \rho(t) \leq 1 \\ P_{\mathrm{sleep}}, & \text{if } \rho(t) = 0 \end{cases}, \tag{1}$$

where P_0 is the power consumption at the minimum non-zero output power, Δ_{p} is the slope of the input-output power consumption, $P_{\max}$ is the maximum output power, and P_{sleep} is the power consumed in sleep mode.

2.2 Energy storage model

We choose a Lithium-ion battery as the power storage device in our architecture for its several advantages such as high energy density and low self-discharge. The battery can store the electricity provided by the PV system and the SG and discharge the stored energy to feed the SBS and sell it back to the SG. In this paper, the battery state is jointly described by its state of charge (SOC) and its state of health (SOH), which both depend on the (dis)charge power. The SOC is an expression of the battery momentary storage level as a percentage of its nominal capacity C_{N} [Ah], which corresponds to the battery capacity at the beginning of life, and the SOH is a metric that reflects the general condition of a battery and its ability to deliver the specified performance compared with a new battery.

2.2.1 State of charge model

The SOC variation is generally calculated using current integration. The rate at which the battery is charged or discharged, noted C_{rate} [s^{-1}], corresponds to the charge or discharge current intensity $i(t)$ [A] relative to the battery nominal capacity:

$$C_{\mathrm{rate}}(t) = \frac{i(t)}{3600 \cdot C_{\mathrm{N}}}. \tag{2}$$

Periodically, for a given C_{rate}, we use the Ampere-Hour integral model to estimate the SOC variation [19]:

$$z(t + \Delta t) = z(t) + \eta \int_{t}^{t+\Delta t} C_{\mathrm{rate}}(u)\mathrm{d}u, \tag{3}$$

where $z(t)$ is the SOC at time t, Δt represents the time step between two SOC estimations, and η is the battery Coulombic efficiency, equals to η_{dis} when discharging and η_{chg} when charging.

2.2.2 Battery power model

The battery is an electrochemical system composed of several modules. Each module is composed of cells organized in series and parallel. Without loss of generality, we suppose that the battery contains n_{s} modules connected in series, where each cell module comprises one cell. In this configuration, the relation between the (dis)charge current $i(t)$ and the voltage of the kth cell V_k [V] is the following [20]:

$$V_k(t) = \mathrm{OCV}(z(t)) + R_k \cdot i(t), \tag{4}$$

where OCV [V] is the open circuit voltage and R_k [Ω] is the kth cell internal resistance, which depends on several parameters such as the SOC, the current intensity, the temperature, and the SOH [21]. The OCV-SOC dependency can be constructed experimentally by disconnecting the battery from any load for a long duration until reaching equilibrium and then measuring its voltage, for different SOC values [22]. The obtained data can be

used to elaborate an analytical OCV model. In this paper, we consider an n-order polynomial approximation model such that [23]:

$$\mathrm{OCV}(z(t)) = \sum_{j=0}^{n} a_j \cdot z^j(t), \tag{5}$$

where n is a natural number and $(a_j)_{j=1..n}$ are the polynomial coefficients calculated from the experimental OCV-SOC dependency function.

As a sign convention, we assume that the charge (resp. discharge) current and power have a positive (resp. negative) sign. Consequently, the power P_{batt} $[W]$ of the battery can be calculated using the sum of all cell power:

$$P_{\mathrm{batt}}(t) = \sum_{k=1}^{n_s} i(t) \cdot V_k(t). \tag{6}$$

By combining Eqs. (2) to (6), the battery power can be expressed as a function of two consecutive SOC values:

$$P_{\mathrm{batt}}(z(t), z(t+\Delta t)) = \sum_{k=1}^{n_s}\sum_{j=0}^{n} A_{j,k} z^j(t) z(t+\Delta t) - B_{j,k}\, z^{j+1}(t) + \alpha^2 \cdot R_k \cdot z^2(t+\Delta t), \tag{7}$$

such that

$$A_{j,k} = \alpha \cdot \left(a_j - 2\alpha \cdot R_k \cdot \delta_{1,j}\right),$$
$$B_{j,k} = \alpha \cdot \left(a_j - \alpha \cdot R_k \cdot \delta_{1,j}\right),$$
$$\alpha = \frac{3600 \cdot C_{\mathrm{N}}}{\eta \cdot \Delta t},$$

and $\delta_{1,j}$ is the Kronecker symbol, equals to 1 when $j = 1$ or 0 otherwise.

2.2.3 State of health models

The SOH degradation is inevitable in a battery life cycle. It is manifested as a loss of available capacity (energy loss) and/or an increase in impedance (power loss). In this paper, we assume that the SOH reflects the capacity evolution:

$$SOH(t) = \frac{C_{\mathrm{ref}}(t)}{C_N}, \tag{8}$$

where $C_{\mathrm{ref}}(t)$ is the reference capacity defined as the battery maximum storage capacity at time t. The degradation of the battery reference capacity can be caused by two aging situations: during use (cycle aging) and on storage (calendar aging) [8]. In the following, these two aging mechanisms are considered independent and thus additive.

Cycle aging: is modeled as reference capacity losses, which depends linearly on the battery SOC variations [24]. At each time step, the new SOH is obtained by Eq. (9):

$$\mathrm{SOH}(t+\Delta t) = \mathrm{SOH}(t) - Z \cdot |\mathrm{SOC}(t) - \mathrm{SOC}(t+\Delta t)|. \tag{9}$$

The experimental results of [25] determine the linear aging coefficient Z for different battery technologies. However, because the cycle aging is amplified outside the recommended operating range $\Delta_{\mathrm{soc}} = [20\%, 90\%]$ of the battery SOC (see Fig. 2 [26]), the aging coefficient Z is defined as:

$$Z = \begin{cases} 85 \times 10^{-6}, & \text{if } 20\% \le \mathrm{SOC}(t) \le 90\% \\ \chi \times 85 \times 10^{-6}, & \text{otherwise} \end{cases} \forall t, \tag{10}$$

where χ is a scalar strictly greater than one.

Calendar aging: The battery temperature is an important parameter to model calendar aging, especially for Li-ion technology. The thermal model is used to estimate the cell temperature in response to the current, voltage,

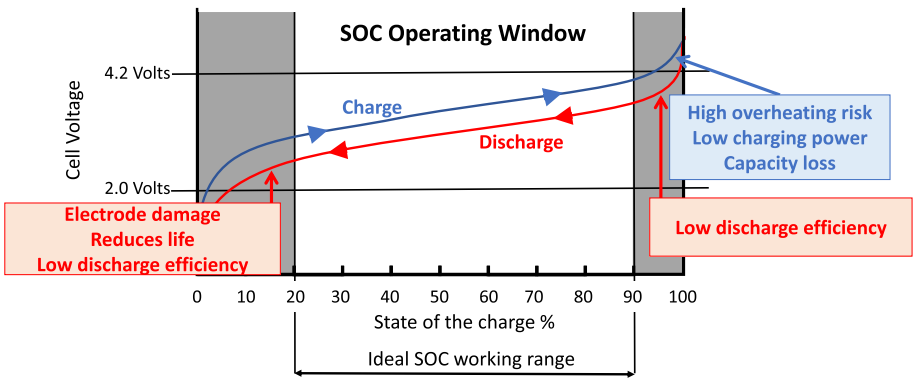

Fig. 2 Recommendations for the operating range of SOC for lithium ion battery [26]

and ambient temperature. According to the energy conservation law, the temperature change for a single-cell battery is given by [27]:

$$m_c \cdot c_h \frac{dT}{dt} = Q_g - Q_r, \tag{11}$$

where m_c [g] is the cell mass, c_h $[J/(g.K)]$ is the specific heat capacity at constant pressure, T [°C] is the temperature within the cell, Q_g $[W]$ is the rate of heat generated by the single cell, and Q_r $[W]$ is the rate of heat removed from the cell by the cooling. The heat generation for a battery cell k can be approximated by Joule heating law:

$$Q_g = R_k \cdot i^2. \tag{12}$$

For simplicity, the heat generation and temperature within the battery are assumed to be uniformly distributed. The single-cell thermal model is thus supposed to represent the overall internal battery temperature.

Ecker et al. [28] have proposed a calendar lifetime prediction model describing the degradation of the battery C_{ref} over time. The model shows exponential dependency with the battery voltage V and temperature T, and square root dependency with the time of rest. The degradation of SOH after a time rest Δt (expressed in weeks) is defined as follows:

$$\frac{\mathrm{SOH}(t+\Delta t)}{\mathrm{SOH}(t)} = 1 + c_a \cdot c_V^{\frac{V-V_0}{\Delta V}} \cdot c_T^{\frac{T-T_0}{\Delta T}} \cdot \sqrt{\Delta t}, \tag{13}$$

where T_0 and V_0 are reference temperature and voltage, ΔT and ΔV are reference temperature and voltage variation, and c_a, c_V, and c_T are fitting parameters based on accelerated calendar aging test data. Given this model, we can conclude that high voltages, and therefore high SOCs (Eq. (4)), contribute to an accelerated battery degradation during rest. Also, the calendar aging grows exponentially with the temperature. Knowing the relation between the current intensity and the heat generated within the battery (Eq. (12)), it is clear that a high current rate increases the internal temperature and therefore leads to faster calendar aging.

2.2.4 Battery aging constraints

The aforementioned aging models suggest that Li-ion batteries must be used within a safe operating area restricted by temperature, current, and SOC windows. Not respecting these restrictions leads to a rapid attenuation of the battery performance (capacity loss and decrease of charge and discharge efficiencies). Also, avoiding a long battery rest duration can considerably lower the calendar aging. In this paper, we consider three aging constraints to preserve the battery from rapid degradations:

- We restrict the battery usage on the specific range of the SOC $\Delta_{SOC} = [20\%, 90\%]$. As discussed earlier, operating the battery outside this range accelerates the cycle aging by factor χ. In addition, the calendar aging is amplified when the battery voltage is high, which corresponds to a high SOC.
- We avoid using high (dis)charge currents that cause accelerated cycle aging (due to deep cycling) and calendar aging (due to heat generation). The current restriction can be reformulated as a limitation of the SOC variation in each decision period:

$$\forall t, \Delta\mathrm{SOC}_{\min} \leq z(t+\Delta t) - z(t) \leq \Delta\mathrm{SOC}_{\max} \tag{14}$$

  where $\Delta\mathrm{SOC}_{\max} \geq 0$ (resp. $\Delta\mathrm{SOC}_{\min} \leq 0$) is the maximum variation of the SOC during charge (resp. discharge).
- We prevent the battery from long resting to lower the calendar aging impact. It is possible to completely avoid rest periods and force the battery into permanent cycling. However, according to some researches [29, 30], providing batteries with a rest period after (dis)charging might be essential for relaxation of gradients generated due to the passage of current and could enable capacity recovery. Such phenomenon is not included in our models, but we can take it into consideration by allowing at most one time step rest between charges and discharges. Equation 15 expresses this constraint by imposing a minimum variation of the SOC (be it positive or negative) over any two consecutive time steps:

$$\forall t, [z(t+2\Delta t) - z(t+\Delta t)]^2 + [(z(t+\Delta t) - z(t)]^2 \geq \epsilon, \tag{15}$$

  where ϵ is strictly positive.

2.3 Harvested energy model

Our architecture uses solar panels to capture solar energy and convert it into electricity via the photo-voltaic (PV) effect. The solar radiation I_g $[W/m^2]$ depends on several factors including geographical location and time of the day.

Let I_t and T_t be the random variables corresponding to the solar radiation and the ambient temperature at hour t, respectively. Given the correlation between the solar radiation and the temperature, we suppose that the combined daily radiation-temperature vector $(I_1, \ldots, I_{24}, T_1, \ldots, T_{24})$ follows a multivariate Gaussian distribution $GP([\boldsymbol{\mu}_{\text{irrad}}, \boldsymbol{\mu}_{\text{temp}}], \boldsymbol{\Sigma}_{\text{irrad-temp}})$, where $\boldsymbol{\mu}_{\text{irrad}}$ (resp. $\boldsymbol{\mu}_{\text{temp}}$) is a vector of size 1×24 composed of the hourly average radiations (resp. temperatures) of the day, and $\boldsymbol{\Sigma}_{\text{irrad-temp}}$ is the covariance matrix 48×48. We compute $\boldsymbol{\mu}_{\text{irrad}}$, $\boldsymbol{\mu}_{\text{temp}}$, and $\boldsymbol{\Sigma}_{\text{irrad-temp}}$ as the means and the covariance of successive realizations related to historical measures of solar radiations and associated temperatures during 5 years [31]. It is noteworthy that by using real historical data, all the phenomena that influence

the temperature and the solar radiation are captured in the obtained stochastic process. Then, the hourly photovoltaic output power P_{PV} [W] is given by the following relation [32]:

$$P_{\mathrm{PV}}(t) = \eta_{\mathrm{PV}} \cdot S \cdot I_{\mathrm{g}}(t), \tag{16}$$

where η_{PV} is the energy conversion efficiency of the solar panel and S [m^2] is the panel surface.

2.4 Energy price model

In the SG, reducing the peak to average consumption ratio is one of the main keys to maintain a smooth balance between the power consumption and production. To this purpose, dynamic pricing can be adopted to adapt consumption profiles to the energy availability.

In this paper, we consider a stochastic dynamic energy price. Let $p(t)$ [\$/kWh] be the random variable corresponding to the buying price (i.e., the cost of energy from the SG) at hour t. The vector $(p(1), \ldots, p(24))$ of daily energy buying price is supposed to follow a multivariate Gaussian distribution $GP(\boldsymbol{\mu}_{\mathrm{price}}, \boldsymbol{\Sigma}_{\mathrm{price}})$, where $\boldsymbol{\mu}_{\mathrm{price}}$ is a vector of size 1×24 composed of the hourly average buying price of the day and $\boldsymbol{\Sigma}_{\mathrm{price}}$ is the covariance matrix 24×24. We compute $\boldsymbol{\mu}_{\mathrm{price}}$ and $\boldsymbol{\Sigma}_{\mathrm{price}}$ as the mean and the covariance of successive realizations related to historical data of electricity pricing for residential customers during 5 years [33]. Moreover, we consider that the price of energy sold to the SG is proportional to the buying price such that $p_{\mathrm{sell}} = \kappa \cdot p$, where κ is the price factor.

3 Cognitive energy supervision system

We aim at minimizing the energy expenditures of the energy-harvesting SBS while reducing the battery aging. This is achieved by scheduling the power flow between the energy sinks and sources over a time horizon discretized into N decision periods. During each time step, we consider that the SBS load, the PV power, and the energy price remain constant. The ESS, in charge of the energy management, is composed of two layers:

1. The high level controller (HLC) schedules the consecutive battery SOCs during the optimization horizon. The obtained energy strategy minimizes the energy cost and reduces the battery aging.
2. The low level controller (LLC) implements the HLC's energy strategy by controlling the power flow between each subsystem in real time such that the energy balance is respected.

Figure 3 represents the cognitive cycle on which the ESS is based. First, the HLC uses the statistical models of the energy variables to solve the long-term (which can be days, hours, or minutes) aging-aware energy cost optimization problem. Specifically, the policy planned by the HLC consists of a succession of the battery SOCs during the optimization period (the SOC variation means that the battery is being charged or discharged, see Section 2.2). Next, according to the SOC strategy, the LLC manages in the short term (minutes to milliseconds) the energy exchange with the SG and between each subsystem of the green small cell. Given the energy conservation law, the LLC senses the realizations of each energy variable and adjusts the power flows to meet the targeted SOC values while respecting the equilibrium between the power supply and demand. In other words, if the energy provided by the PV system and/or the battery is not sufficient to power the SBS and/or the battery, the LLC purchases the missing quantity from the SG. Similarly, the LCC sells the energy surplus when the provided energy exceeds the consumption.

This study focuses on the HLC. We suppose that the LLC is available and operates in real time. The constrained cost optimization problem $\mathbf{P_1}$ at the HLC level aims to find the optimal SOC strategy $\mathbf{z}^* = (z^*(1), \ldots, z^*(N+1))$ and is defined as follows:

$$\mathbf{P}_1 : \underset{(z(1),\ldots,z(N+1)) \in [0,1]^{N+1}}{\operatorname{argmin}} \sum_{t=1}^{N} p(t) \cdot [E_b(t) + \kappa E_s(t)],$$

subject to

$$E_b(t) = \max\left(0, P_{\mathrm{BS}}(t) + P_{\mathrm{Batt}}(z(t), z(t+1)) - P_{\mathrm{PV}}(t)\right), \tag{17}$$

$$E_s(t) = \min\left(0, P_{\mathrm{BS}}(t) + P_{\mathrm{Batt}}(z(t), z(t+1)) - P_{\mathrm{PV}}(t)\right), \tag{18}$$

$$z(t) \in \Delta_{\mathrm{SOC}}, t = 1, \ldots, N+1, \tag{19}$$

$$\Delta SOC_{\min} \leq z(t+1) - z(t) \leq \Delta SOC_{\max}, t = 1, \ldots, N, \tag{20}$$

$$[z(t+2) - z(t+1)]^2 + [(z(t+1) - z(t)]^2 \geq \epsilon, t = 1, \ldots, N-1, \tag{21}$$

where $(z(1), \ldots, z(N+1))$ is the decision vector that represents the battery SOCs over the optimization horizon and $E_b \geq 0$ (resp. $E_s \leq 0$) is the amount of energy bought from (resp. sold to) the SG. The objective function of $\mathbf{P_1}$ corresponds to the long-term cost due to power transactions with the electrical grid. At all time steps, the balance between the power supply and demand is illustrated by the constraints (Eqs. (17) and (18)). Note that the battery can be either an energy source (when $P_{\mathrm{Batt}}(z(t), z(t+1)) \leq 0$) or a load (when $P_{\mathrm{Batt}}(z(t), z(t+1)) \geq 0$). When the

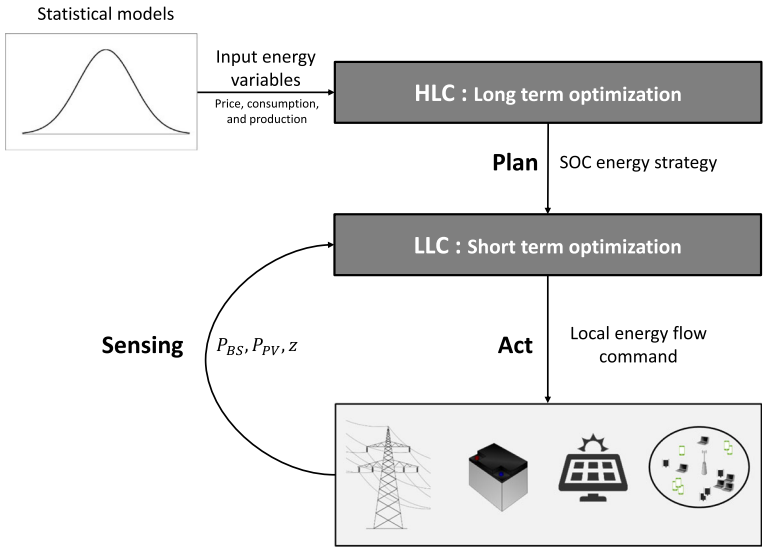

Fig. 3 Proposed cognitive energy supervision infrastructure

energy consumed is greater than the energy provided by the PV/battery system (i.e., $P_{\mathrm{BS}}(t) + P_{\mathrm{Batt}}(z(t), z(t+1)) - P_{\mathrm{PV}} \geq 0$), the controller perceives a cost $p(t) \cdot E_b(t) \geq 0$ corresponding to the energy bought from the SG. In contrast, when the energy available is superior to the energy consumption (i.e., $P_{\mathrm{BS}}(t) + P_{\mathrm{Batt}}(z(t), z(t+1)) - P_{\mathrm{PV}} \leq 0$), the controller receives a negative cost $\kappa p(t) \cdot E_s(t) \leq 0$ (that can be seen as a reward) associated with the energy sold to the SG. The aim of the HLC is to jointly minimize the cumulative positive costs and maximize the cumulative rewards, which corresponds to minimize the negative costs. In addition, during all the decision periods, Eqs. (19), (20), and (21) represent the constraints on the SOC that have to be respected to improve the battery life span (see Section. 2.2.4).

4 Results and discussion

The simulation has been accomplished for finite horizons of 24 h, that is $N = 24$ and $\Delta_t = 1$ h. The stochastic variables are generated each hour of the day according to their respective models. The profiles illustrated in Fig. 4 describe the hourly average SBS load, solar radiation, ambient temperature, and energy buying price used in our simulations to model the average SBS load ρ, the average solar radiation $\boldsymbol{\mu}_{\mathrm{irrad}}$, the average ambient temperature $\boldsymbol{\mu}_{\mathrm{temp}}$, and the average energy buying price $\boldsymbol{\mu}_{\mathrm{price}}$, respectively. Regarding the SBS, the general trend is a progressive increase of the traffic load such that the peak is reached around 21:00–22:00. Notice that the load between 3:00 and 10:00 is absent since it is completely handled by the under-layer macro base station. Concerning the solar

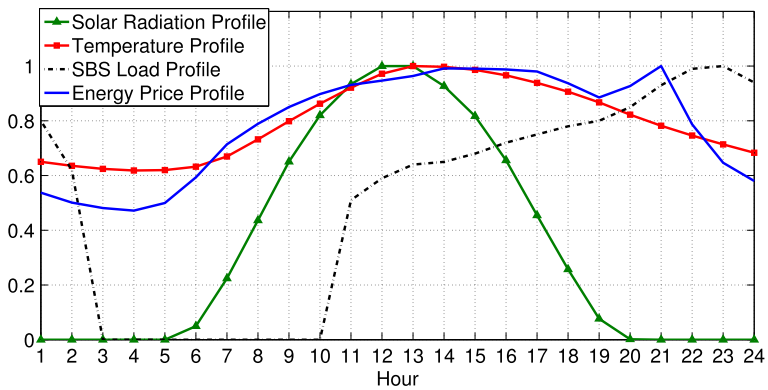

Fig. 4 Normalized profiles of the average solar radiation, average ambient temperature [31], SBS load (based on [36]), and average energy price [33]

Table 1 Simulation parameters

	Parameter	Value	Parameter	Value
SBS	P_0	13.6 W	Δ_p	4
	P_{max}	0.13 W	P_{sleep}	8.6 W
Battery	n_s	5	C_N	7 Ah
	$\forall k\ R_k$	50 mΩ	η_{chg}	96%
	η_{dis}	100%	z_0	30%
	ΔSOC_{min}	−30%	ΔSOC_{max}	30%
	ϵ	10^{-4}		
Solar panel	η_{PV}	14%	S	0.25 m^2
Energy price	κ	100%		

Table 2 Battery thermal and aging simulation parameters [28, 35]

Parameter	Value	Parameter	Value
c_h	1900 J/(kg K)	V_0	3.5 V
c_a	−0.0064	T_0	25 °C
c_V	1.1484	ΔV	0.1 V
c_T	1.5479	ΔT	10 °C
χ	5	m_c	40g

radiation and ambient temperature, the profiles are both bell-shaped and the peak is reached around midday. In particular, the solar radiation is available only at daytime. Finally, the SG electricity price is characterized by two separated peak hours (between 14:00–16:00 and at 21:00) and off-peak intervals during night and evening.

We also consider our experimental data for Li-ion batteries to model the OCV (Eq. (5)) as a second order polynomial such that $OCV(z(t)) = 2.9 + 0.13 \cdot z(t) - 0.008 \cdot z^2(t)$. Other simulation settings for each component of the system are summarized in Tables 1 and 2. Without loss of generality, we assume that the battery parameters (nominal capacity, cell resistance, and charge/discharge efficiency) are independent of the current intensity and temperature. Also, it is noteworthy that the usage of the hour as a time step does not lead to loss of generality. In reality, we can consider another time scale (e.g., minutes) for the power control and the dynamics of the energy variables without any further changes in the energy management framework.

In this paper, we adopt an offline approach to solve the non-linear constrained problem $\mathbf{P_1}$. We suppose that the ESS operates in the *ideal* case where the realizations of the SBS load, solar radiation, temperature, and energy price over all the optimization period are considered known. By doing so, we can assess the ESS maximum performance, which can serve as an upper bound in the realistic case where the stochastic variables cannot be perfectly forecast. In this configuration, the simulation has been performed for 1825 different days (5 years), such that $\mathbf{P_1}$ is solved each 24 h by running the interior-point algorithm implemented in MATLAB with several initializations to reduce the probability of local minima [34]. Furthermore, we evaluate the trade-off between the SBS energy opex savings and the battery life span preservation by solving $\mathbf{P_1}$ considering three constraint sets:

1. $\mathcal{C}_1$ = {Eqs. (17) and (18)}. The decision-making does not take into consideration the battery life span preservation.
2. $\mathcal{C}_2$ = {Eqs. (17) to (20)}. The power flow strategy includes as constraints the recommended battery operating SOC interval and maximum (dis)charge rate.
3. $\mathcal{C}_3$ = {Eqs. (17) to (21)}. In addition to the recommended battery operating SOC interval and maximum (dis)charge rate, the power flow strategy includes the battery rest time limitation.

The results obtained for each 24 h are averaged and presented in the following subsections.

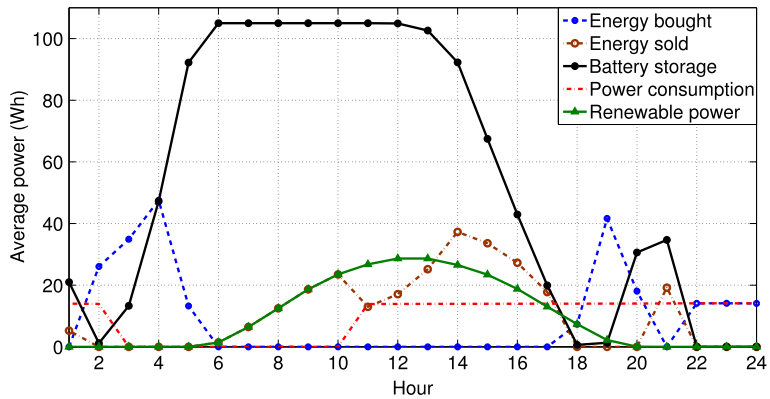

Fig. 5 Energy transaction, consumption, production, and storage with the *ideal* strategy under $\mathcal{C}_1$, averaged over 5 years

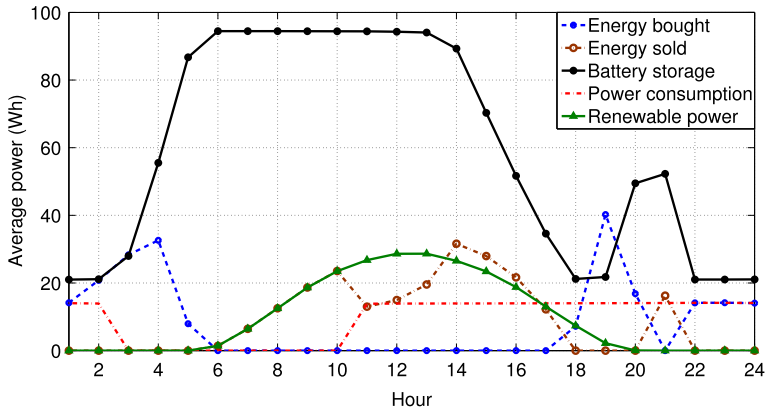

Fig. 6 Energy transaction, consumption, production, and storage with the *ideal* strategy under $\mathcal{C}_2$, averaged over 5 years

4.1 Power flow management

The energy flows obtained under the constraint sets $\mathcal{C}_1$, $\mathcal{C}_2$, and $\mathcal{C}_3$ are respectively presented in Figs. 5, 6, and 7. In these figures, we have represented the average SBS energy consumption, RE production, energy transactions with the SG, and energy stored in the battery. We observe that, in average, the cognitive ESS buys electricity at night, when the PV system cannot produce any energy, to power the SBS and/or store it into the battery. Additionally, we can note that the amount of energy purchased from the SG depends closely on the energy price (the lower the price, the higher the amount of energy bought). Once the PV production becomes available or when the price is high, the cognitive ESS prioritizes the use of the energy produced by the PV panel and the energy already stored in the battery to feed the SBS and sells a quantity of the surplus to the SG. Note that the global behavior of the three policies is similar. However, there are some differences between these strategies, generated by the battery constraints imposed in each case. In $\mathcal{C}_1$ (Fig. 5), the absence of any battery operational limitations enables the ESS to charge and discharge the battery at full (from 0 Wh to 105 Wh), using high (dis)charge current intensities (for example, the SOC variation between 4:00 and 5:00 is equal to $45\% \geq \Delta\text{SOC}_{\max}$). Some limitations are introduced in $\mathcal{C}_2$ (Fig. 6) such that the SOC values are restricted in Δ_{SOC} (corresponding to the battery power level interval [20, 95] Wh), and all the SOC variations are limited between $\Delta\text{SOC}_{\min}$ and $\Delta\text{SOC}_{\max}$. Finally, $\mathcal{C}_3$ (Fig. 7) includes $\mathcal{C}_2$ constraints in addition to the calendar aging restriction that avoid a long battery inactivity. For example, and contrarily to $\mathcal{C}_2$, slight battery (dis)charges have been introduced between 7:00 and 13:00 to generate a battery activity and prevent large capacity losses due to the calendar aging process.

Figure 8 compares the *ideal* strategy under each constraint sets. The battery power flow under the constraint set $\mathcal{C}_1$ is characterized by high battery currents and extreme SOCs. The amounts of energy exchanged with the SG are large and the battery state varies rapidly. In contrast, the strategies under $\mathcal{C}_2$ and $\mathcal{C}_3$ involve progressive battery (dis)charge such that the aging constraints are

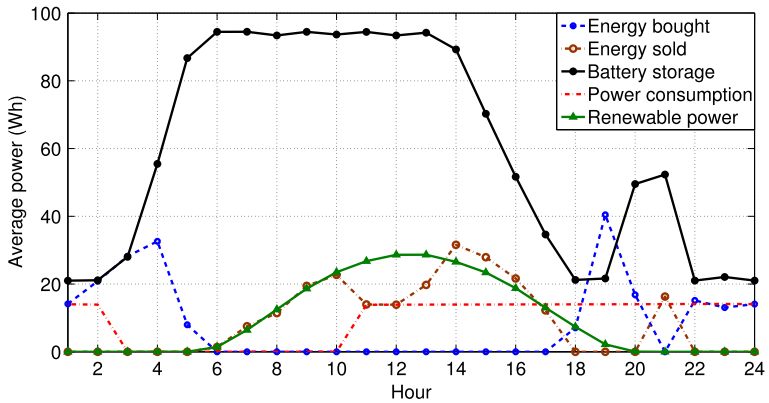

Fig. 7 Energy transaction, consumption, production, and storage with the *ideal* strategy under $\mathcal{C}_3$, averaged over 5 years

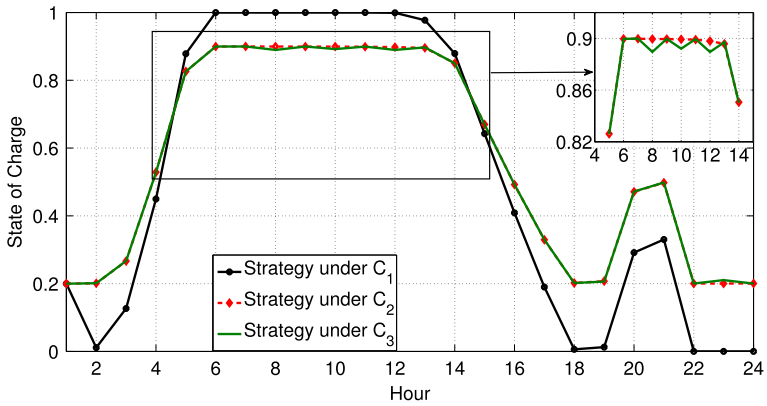

Fig. 8 Average SOC of the *ideal* strategy under the constraint sets $\mathcal{C}_1$, $\mathcal{C}_2$, and $\mathcal{C}_3$

respected. In reality, these two strategies are very similar such that the only differences are noticed between 7:00–13:00 and 22:00–0:00 regarding the battery storage level and the energy bought from the grid. This difference is due to Eq. (21), which restricts the battery rest during two consecutive time steps and generates a sawtooth pattern with respect to the SOC.

4.2 Battery aging

In this section, we investigate the impact of each power scheduling policy on the battery aging. As mentioned before, such aging phenomenon can be dissociated into two parts: the cycle aging and the calendar one.

Figure 9 shows the average time evolution of the SOH due to cycle aging for the ideal strategy in the three constraint configurations. Each time the battery is charged or discharged, the cycle aging contributes to decrease its life span whereas no degradation occurs during rest. The battery degradation observed under $\mathcal{C}_1$ (0.08% SOH loss per day) are substantially high compared to the strategy under $\mathcal{C}_2$ and $\mathcal{C}_3$ (0.02% SOH loss per day). The accelerated aging is explained by the profound depth of (dis)charge cycles and the battery operating in dangerous SOC areas (below 20% and above 90%). Besides, the cycle aging in $\mathcal{C}_3$ is slightly higher than $\mathcal{C}_2$ because of the additional cycling that prevent long battery rests.

Similarly, Fig. 10 illustrates the battery calendar aging in the three constraint configurations. The calendar aging corresponds to the SOH loss when the battery is not used and depends on the rest duration, momentary voltage, and temperature. In the unconstrained case $\mathcal{C}_1$, the internal battery temperature peaks illustrated in Fig. 11 are caused by deep battery (dis)charges. The corresponding current intensities are such high that the generated heat by Joule effect increases the battery internal temperature to attain large values (30 °C). In this situation, the accumulated calendar aging can also be considerable (0.12% SOH loss in 1 day). The SOC constraints $\mathcal{C}_2$ contribute to slightly reduce the impact of the calendar aging process thanks to current and voltage limitations (0.09% per day). However, it is only by restricting the rest time, such as we do by introducing $\mathcal{C}_3$, that calendar aging can be considerably avoided (0.02% per day).

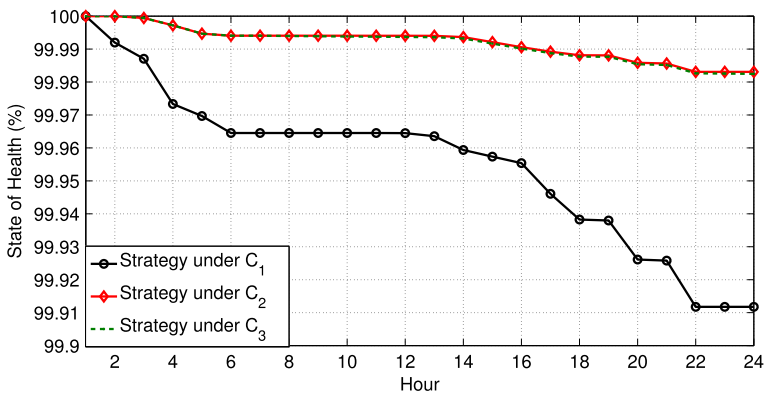

Fig. 9 Average battery cycle aging of the *ideal* strategy under the constraint sets $\mathcal{C}_1$, $\mathcal{C}_2$, and $\mathcal{C}_3$

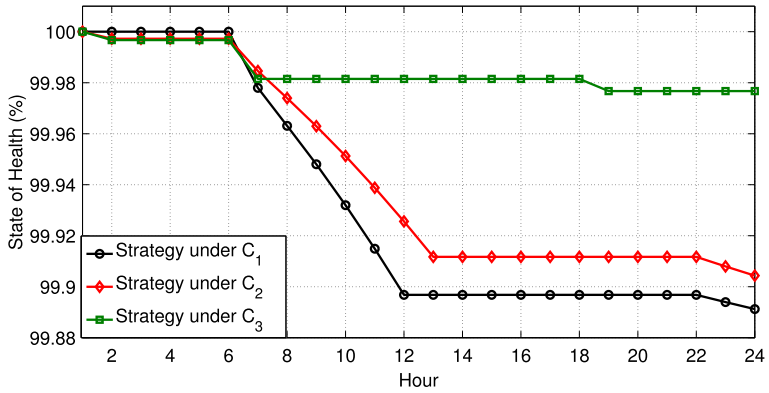

Fig. 10 Average battery calendar aging of the *ideal* strategy under the constraint sets $\mathcal{C}_1$, $\mathcal{C}_2$, and $\mathcal{C}_3$

Finally, by summing the cycle and calendar aging effects, we conclude that the respect of the SOC constraints enables considerable reduction of the battery degradation rate. This allows in average 51% (resp. 30%) of the battery SOH preservation per year when operating under $\mathcal{C}_3$ (resp. $\mathcal{C}_2$) compared to the unconstrained case $\mathcal{C}_1$.

4.3 Economic performance

In this part, we assess the economic performance of the proposed energy management by comparing the energy cost of the ideal strategy with two other schemes:

1. The *reference strategy* that systematically buys all the energy needed to feed the SBS from the SG. The battery and the PV system are not used.
2. The *naive strategy* is a greedy strategy that aims to decrease the immediate energy cost, regardless of any long-term cost saving opportunity. At each decision period, the PV production is first dedicated to cover the SBS consumption. In case the production exceeds the consumption, the surplus is sold to the SG. Otherwise, the missing energy is purchased from the SG. Consequently, the battery is never used.

For this analysis, we assume a battery investment cost of \$0.4/Wh that includes the purchase and installation fees. Figure 12 represents the normalized average hourly cost of the ideal (under the three constraint sets), naive and, reference strategies. In the reference strategy, the cost is exclusively generated by the SBS consumption. Once the PV production is considered, it appears that the naive strategy overlaps with the reference strategy during night, while energy production during day is sufficient to feed the SBS and sell energy back to the SG (negative cost). Concerning the ideal strategy, we first notice the energy purchase used to charge the battery during time intervals that match with off-peak price periods. The energy stored is then discharged when the electricity price is high to achieve a higher benefit compared to the aforementioned strategies. In particular, the ideal strategy under $\mathcal{C}_1$ spends and earns more than those under $\mathcal{C}_2$ and $\mathcal{C}_3$ given the additional allowed battery flexibility.

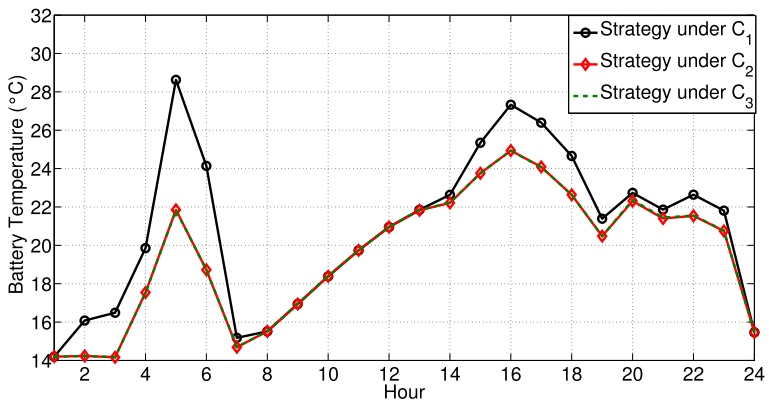

Fig. 11 Average battery temperature of the *ideal* strategy under the constraint sets $\mathcal{C}_1$, $\mathcal{C}_2$, and $\mathcal{C}_3$

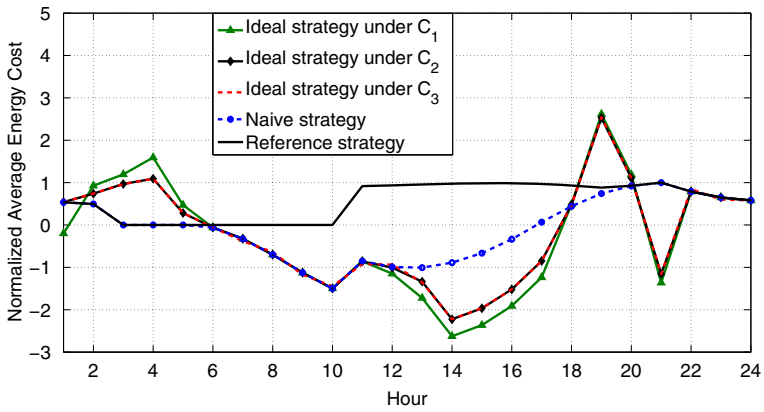

Fig. 12 Normalized daily energy cost of the *ideal* (under $\boldsymbol{\mathcal{C}}_1$, $\boldsymbol{\mathcal{C}}_2$, and $\boldsymbol{\mathcal{C}}_3$), the *naive*, and the *reference* strategies, averaged over 5 years

Table 3 shows the accumulated energy costs averaged over 5 years and normalized with respect to the reference policy. Negative costs mean that not only cost saving is achieved but also the mobile operator is making profits. The largest cost saving of 145% compared to the reference is naturally achieved in the ideal case under $\mathcal{C}_1$. With the constraints $\mathcal{C}_2$ and $\mathcal{C}_3$, the proposed cognitive energy management framework performs approximately 132% cost reduction. On the contrary, the naive strategy achieves only one quarter of the ideal strategy cost savings.

It is clear that an efficient use of the battery enables more flexibility in the energy trading. In fact, the ESS can exploit the price variation to buy energy at low cost, not only to match an imminent energy demand but also to store it in prevision of future consumption that can generate heavy expenditures from the SG. Also, the RE energy can be saved in the battery until interesting selling prices are offered by the SG. However, there is a trade-off between how much the battery can be used to realize cost savings and the aging issues. In fact, when the battery aging constraints ($\mathcal{C}_2$ and $\mathcal{C}_3$) are respected, the cost saving is reduced by about ten points, which corresponds to a loss of \$1.6 in 1 year. At the same time, 30% (resp. 51%) of the battery initial SOH is preserved per year, equivalent to \$13 (resp. \$20) cost saving each year under $\mathcal{C}_2$ (resp. $\mathcal{C}_3$), which is by far more profitable given the current battery cost. In other words, it means that the implementation of the ideal energy strategy requires the battery replacement after 1.5 years under $\mathcal{C}_1$, 3 years under $\mathcal{C}_2$, and 7 years under $\mathcal{C}_3$.

Table 3 Normalized average opex for the *ideal* (with and without SOC constraints), *naive*, and *reference* strategies

Strategy	Ideal under $\boldsymbol{\mathcal{C}}_1$	Ideal under $\boldsymbol{\mathcal{C}}_2$	Ideal under $\boldsymbol{\mathcal{C}}_3$	Naive	Reference
Cost	−0.45	−0.332	−0.329	−0.11	1

5 Conclusions

In this paper, we have presented a cognitive energy controller for a small cell base station connected to the smart grid and equipped with a battery and renewable production. This architecture had for purpose to jointly optimize the energy cost and reduce the battery aging effects. Obtained simulation results have shown that the energy supervision system achieves very large cost reduction compared to basic strategies while enhancing the storage life span. In particular, the battery aging constraints allows to considerably reduce the calendar and cycle degradation (up to 51% in average of the initial state of health preserved per year). Furthermore, the respect of these constraints resulted in only ten points decrease of the average opex cost saving, which is negligible considering current battery costs. As future work, we plan to study the proposed cognitive energy supervision framework considering casual information about the environment energy variable. We also aim to realize a demonstrator of the proposed solution to assess its performances in real-life conditions.

Funding
The research leading to these results is funded by the French Agence Nationale de la Recherche in the framework of the SOGREEN project (ANR-14-CE29-0025-01).

Authors' contributions
MM, ADeD, VH, RC, and NH substantially contributed to the conception or design of the work or the acquisition, analysis, or interpretation of data for the work. MM, ADeD, and VH drafted the work and revised it critically for important intellectual content. MM, ADeD, VH, RC, and NH agreed to be accountable for all aspects of the work in ensuring that questions related to the accuracy or integrity of any part of the work are appropriately investigated and resolved. MM, ADeD, VH, RC, and NH contributed to the final approval of the version to be published.

Competing interests
The authors declare that they have no competing interests.

Publisher's Note

Received: 11 November 2016 Accepted: 6 July 2017
Published online: 18 July 2017

References

1. Small Cells Deployment Market Status 2015 Report. http://scf.io. Accessed 20 Feb 2016
2. HAH Hassan, L Nuaymi, A Pelov, in *Online Conference on Green Communications (GreenCom), 2013 IEEE*. Renewable energy in cellular networks: a survey (IEEE, 2013), pp. 1–7
3. A De Domenico, E Calvanese Strinati, A Capone, Enabling green cellular networks: a survey and outlook. Comput. Commun. **37**, 5–24 (2014)
4. G Piro, M Miozzo, G Forte, N Baldo, LA Grieco, G Boggia, P Dini, HetNets powered by renewable energy sources: sustainable next-generation cellular networks. IEEE. Internet Comput. **17**(1), 32–39 (2013)
5. H Wang, H Li, C Tang, L Ye, X Chen, H Tang, S Ci, Modeling, metrics, and optimal design for solar energy-powered base station system. EURASIP J. Wirel. Commun. Netw. **2015**(1), 39 (2015)
6. J Palicot, in *Proceedings of the 2009 International Conference on Wireless Communications and Mobile Computing: Connecting the World Wirelessly*. Cognitive radio: an enabling technology for the green radio communications concept (ACM, 2009), pp. 489–494
7. S Jin, X Ma, W Yue, Energy-saving strategy for green cognitive radio networks with an LTE-advanced structure. J. Commun. Netw. **18**(4), 610–618 (2016)
8. M Broussely, P Biensan, F Bonhomme, P Blanchard, S Herreyre, K Nechev, RJ Staniewicz, Main aging mechanisms in li-ion batteries. J. Power Sources. **146**(1-2), 90–96 (2005)
9. A Barré, B Deguilhem, S Grolleau, M Gérard, F Suard, D Riu, A review on lithium-ion battery ageing mechanisms and estimations for automotive applications. J. Power Sources. **241**, 680–689 (2013)
10. N Michelusi, L Badia, R Carli, L Corradini, M Zorzi, Energy management policies for harvesting-based wireless sensor devices with battery degradation. IEEE Trans. Commun. **61**, 4934–4947 (2013)
11. C Liu, B Natarajan, Power management in heterogeneous networks with energy harvesting base stations. Phys. Commun. **16**(C), 14–24 (2015)
12. S Zhang, N Zhang, S Zhou, J Gong, Z Niu, X Shen, Energy-aware traffic offloading for green heterogeneous networks. IEEE J. Selected Areas Commun. **34**(5), 1116–1129 (2016)
13. R Kaewpuang, D Niyato, P Wang, Decomposition of stochastic power management for wireless base station in smart grid. IEEE Wirel. Commun. Lett. **1**(2), 97–100 (2012)
14. J Leithon, TJ Lim, S Sun, in *Smart Grid Communications (SmartGridComm), 2013 IEEE International Conference on*. Online energy management strategies for base stations powered by the smart grid (IEEE, 2013), pp. 199–204
15. Y Mao, J Zhang, KB Letaief, Grid energy consumption and QoS tradeoff in hybrid energy supply wireless networks. IEEE Trans. Wirel. Commun. **15**(5), 3573–3586 (2016)
16. M Mendil, A De Domenico, V Heiries, R Caire, N Hadj-said, in *Personal, Indoor, and Mobile Radio Communications (PIMRC), 2016 IEEE 27th Annual International Symposium on*. Fuzzy Q-learning based energy management of small cells powered by the smart grid (IEEE, 2016), pp. 1–6
17. M Mendil, A De Domenico, V Heiries, R Caire, N Hadj-said, in *International Conference on Cognitive Radio Oriented Wireless Networks*. Energy management of green small cells powered by the smart grid (Springer, 2016), pp. 642–653
18. G Auer, V Giannini, C Desset, EA Godor, How much energy is needed to run a wireless network? IEEE Wirel. Commun. **18**(5), 40–49 (2011)
19. L Lu, X Han, J Li, J Hua, M Ouyang, A review on the key issues for lithium-ion battery management in electric vehicles. J. Power Sources. **226**, 272–288 (2013)
20. R Restaino, W Zamboni, in *IECON 2012-38th Annual Conference on IEEE Industrial Electronics Society*. Comparing particle filter and extended kalman filter for battery state-of-charge estimation (IEEE, 2012), pp. 4018–4023
21. A Barre, F Suard, M Gérard, M Montaru, D Riu, Statistical analysis for understanding and predicting battery degradations in real-life electric vehicle use. J. Power Sources. **245**, 846–856 (2014)
22. W-Y Chang, The state of charge estimating methods for battery: a review. ISRN Appl. Math. **2013**, 1–7 (2013)
23. C Weng, J Sun, H Peng, in *ASME 2013 dynamic systems and control conference*. An open-circuit-voltage model of lithium-ion batteries for effective incremental capacity analysis (American Society of Mechanical Engineers, 2013), pp. V001T05A002–V001T05A002
24. Y Riffonneau, S Bacha, F Barruel, S Ploix, Optimal power flow management for grid connected PV systems with batteries. IEEE Trans. Sustainable Energy. **2**(3), 309–320 (2011)
25. E Lemaire-Potteau, F Mattera, A Delaille, P Malbranche, in *23rd European Photovoltaic Solar Energy Conference (Valencia, Spain, 2008)*. Assessment of storage ageing in different types of PV systems: technical and economical aspects, (Valencia, 2008), pp. 2765–2769
26. Lithium battery failures. http://www.mpoweruk.com/lithium_failures.htm. Accessed 20 Feb 2016
27. A Cordoba-Arenas, S Onori, G Rizzoni, A control-oriented lithium-ion battery pack model for plug-in hybrid electric vehicle cycle-life studies and system design with consideration of health management. J. Power Sources. **279**, 791–808 (2015)
28. M Ecker, JB Gerschler, J Vogel, S Käbitz, F Hust, P Dechent, DU Sauer, Development of a lifetime prediction model for lithium-ion batteries based on extended accelerated aging test data. J. Power Sources. **215**, 248–257 (2012)
29. A Eddahech, O Briat, J-M Vinassa, Lithium-ion battery performance improvement based on capacity recovery exploitation. Electrochimica Acta. **114**, 750–757 (2013)
30. M Rashid, A Gupta, Effect of relaxation periods over cycling performance of a li-ion battery. J. Electrochem. Soc. **162**(2), 3145–3153 (2015)
31. G SOLAR, Solar radiation time series. http://geomodelsolar.eu/data/full-time-series. Accessed 20 Feb 2016
32. G Rami, T Tran-Quoc, N Hadjsaid, JL Mertz, in *Power Engineering Society General Meeting, 2004. IEEE*. Energy supply for remote base transceiver stations of telecommunication (IEEE, 2004), pp. 1916–1921
33. Ameren: Ameren price database. https://www2.ameren.com/RetailEnergy/rtpDownload. Accessed 20 Feb 2016
34. A Forsgren, PE Gill, MH Wright, Interior methods for nonlinear optimization. SIAM Rev. **44**(4), 525–597 (2002)
35. K Uddin, A Picarelli, C Lyness, N Taylor, J Marco, An acausal li-ion battery pack model for automotive applications. Energies. **7**(9), 5675–5700 (2014)
36. G Auer, O Blume, V Giannini, I Godor, M Imran, Y Jading, E Katranaras, M Olsson, D Sabella, P Skillermark, *et al*, D2. 3: Energy efficiency analysis of the reference systems, areas of improvements and target breakdown. EARTH. **20**(10) (2010)